Membrane Tilt Drives Phase Separation of Adhesion Receptors

Shao-Zhen Lin,[1] Rishita Changede,[2,3] Aaron J. Farrugia,[2] Alexander D. Bershadsky,[4,2] Michael P. Sheetz,[2,5] Jacques Prost,[6,2,*] and Jean-François Rupprecht[1,†]

[1]*Aix Marseille Univ, Université de Toulon, CNRS, CPT (UMR 7332), Turing Centre for Living Systems, Marseille, France*
[2]*Mechanobiology Institute, National University of Singapore, 117411 Singapore*
[3]*TeOra Pte Ltd, Singapore, Singapore*
[4]*Department of Molecular Cell Biology, Weizmann Institute of Science, Israel*
[5]*Biochemistry and Molecular Biology Department, University of Texas Medical Branch, Galveston, Texas 77555, USA*
[6]*Laboratoire Physico-Chimie Curie, UMR 168, Institut Curie, PSL Research University, CNRS, Sorbonne Université, 75005 Paris, France*

(Received 31 August 2023; accepted 25 March 2024; published 3 May 2024)

Cell adhesion receptors are transmembrane proteins that bind cells to their environment. These proteins typically cluster into disk-shaped or linear structures. Here, we show that such clustering patterns spontaneously emerge when the receptor senses the membrane deformation gradient, for example, by reaching a lower-energy conformation when the membrane is tilted relative to the underlying binding substrate. Increasing the strength of the membrane gradient-sensing mechanism first yields isolated disk-shaped clusters and then long linear structures. Our theory is coherent with experimental estimates of the parameters, suggesting that a tilt-induced clustering mechanism is relevant in the context of cell adhesion.

DOI: 10.1103/PhysRevLett.132.188402

Introduction.—Clusters of cell adhesion receptors play a critical role as signaling platforms regulating tissue integrity [1–5], antigen recognition by immune cells [6], and neuronal connections [7].

Here, we propose a generic model for the clustering of cell adhesion receptors upon interactions with a flat, rigid substrate. Our approach is in the same spirit as the pioneering work of Bruinsma and Sackmann [8], but we take an explicit account of the conformation of binding receptors upon binding. In particular, we consider the case of a binder that tends to tilt to both the membrane and the substrate with angles denoted θ_i and δ_i, respectively, as shown in Fig. 1(a). This results in the membrane tilting to the substrate upon binding (see also Ref. [9], Fig. 8).

Considering such a tilt effect, we show that a characteristic cluster size emerges and that no ripening takes place. This contrasts with previous work on the subject [10,11], which considered clustering as a nucleation problem and focused on determining the critical size beyond which clusters would continuously grow.

Our model predicts that clusters of receptors can form as circular dots or long linear structures depending on the tilt-induced negative surface tension and the membrane-substrate adhesion. This is echoed by experiments, with nascent adhesions displaying circular clusters with 100 nm diameter [12,13], and fibrillar adhesions displaying micron-long linear structures that are mediated by a5b1 integrin and enriched in Tensin3 [14,15] (see also Fig. 3).

Our Letter is organized as follows: We first present the model, show the analytic and numerical results, and discuss experimental agreement.

Model.—Our model relies on two fields: $\phi(\boldsymbol{x}) \in (0,1)$, the fraction of bound cell adhesion receptors among other molecules, and $e(\boldsymbol{x})$ measures the height of the membrane with respect to the substrate; see Figs. 1(a) and 1(b).

We consider a total free energy for the membrane-receptor-substrate system in the form $F[e,\phi] = F_{\mathrm{FH}}[\phi] + F_{\mathrm{Hel}}[e] + F_{\mathrm{int}}[e,\phi]$, where F_{FH} accounts for an entropy of mixing (which depends on ϕ only), F_{Hel} for the mechanical energy of membrane deformation (which depends on e only), and $F_{\mathrm{int}}[e,\phi] = F_{\mathrm{tilt}}[e,\phi] + F_{\mathrm{adh}}[e,\phi]$ for tilt and adhesion-based interactions which, in our model, will couple the ϕ and e fields. We find that $F_{\mathrm{FH}} = \int \mathrm{d}^2\boldsymbol{x}\{(k_BT/a)[\phi\ln\phi + (1-\phi)\ln(1-\phi)] + D_\phi(\nabla\phi)^2/2\}$ (see Supplemental Material [16], Sec. I), where k_BT is the thermal energy (as in Flory-Huggins theory [25,26]), a is the inverse areal density of binders, D_ϕ is a gradient energy coefficient that controls the width of the interface of the bound receptor clusters [27], and the integral is over an entire domain of interest, which corresponds to a region within the bulk of the adhered region (e.g., away from the cell edge by a few hundred nanometers). We model the membrane through the classical Helfrich free energy [28,29], $F_{\mathrm{Hel}} = \int \mathrm{d}^2\boldsymbol{x}[\sigma(\nabla e)^2/2 + \kappa(\nabla^2 e - c_0)^2/2]$, where σ is the surface tension, κ the bending stiffness, and c_0 the spontaneous curvature of the membrane.

Tilt.—We propose that the average conformation of bound receptors is affected by the local *gradient* in the membrane height.

We first illustrate our model by considering an imposed binder-membrane angle statistics $\vec{\theta}_i = \pm\theta_0\vec{x}$; see Fig. 1(a).

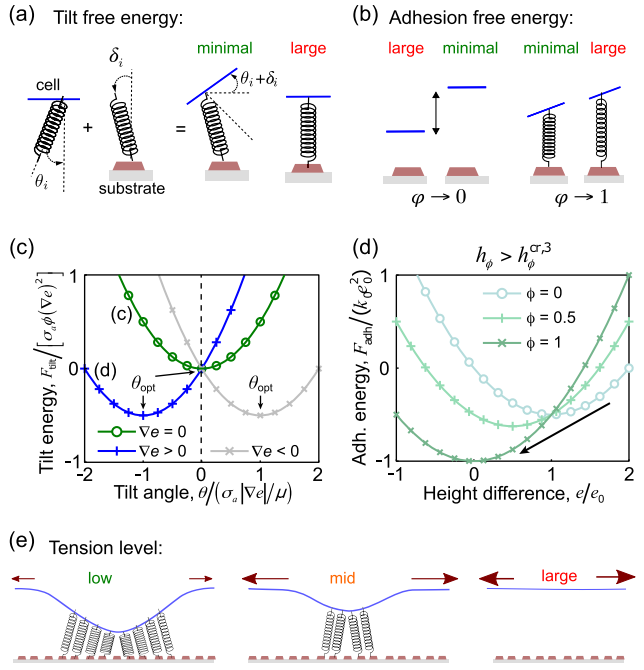

FIG. 1. (a) Tilted binders with respect to the membrane (angle θ_i) and substrate (angle δ_i). The tilt free energy is then minimized when the membrane is inclined to the substrate; membrane (blue), cell adhesion receptors (black, springs), ligands (red), and substrate (gray). (b) Membrane-receptor-substrate adhesion free energy cost in the absence (left, $\phi = 0$) and in the case of full occupancy by binders (right, $\phi = 1$). (c) The tilt free energy $F_{\rm tilt}$ [see Eq. (1)] as a function of the average tilt angle $\theta = \langle\theta_i\rangle$, at given values of ∇e (1D case). (d) The adhesion energy $F_{\rm adh}$ [see Eq. (4)] as a function of the normalized height difference e/e_0 in the case $h_\phi > h_\phi^{\rm cr,3}$, for homogeneous states. A black arrow indicates a shift from a fully detached state ($\phi = 0$) to a fully attached state ($\phi = 1$). (e) Clustering sketch for different levels of membrane tension in the case $h_\phi < h_\phi^{\rm cr,3}$.

Considering an elastic energy on the binder-substrate angle results in $E_i = K(\theta_i + \nabla e)^2/2$; the Boltzmann average tilt then simply reads $\vec{\theta} = \langle\vec{\theta}_i\rangle = -[(K\theta_0^2)/(k_BT)]\vec{\nabla}e$ (see Supplemental Material [16], Sec. II).

In the following, we consider a minimal and generic description that encompasses such an onset of local polar order, denoted $\vec{\theta}(\vec{x})$ and called average tilt. The presence of a height gradient breaks the symmetry and allows for the emergence of a nonzero average tilt vector $\vec{\theta}(\vec{x}) = \langle\vec{\theta}_i\rangle \neq 0$ [Figs. 1(a) and 1(c)]. The statistics of such an average tilt vector can be described through the free energy

$$F_{\rm tilt} = \int {\rm d}^2\boldsymbol{x}\phi(\boldsymbol{x})\left[\mu\vec{\theta}\cdot\vec{\nabla}e + \frac{\nu}{2}\vec{\theta}^2\right], \tag{1}$$

where μ and ν define the average tilt angle minimizing the free energy:

$$\vec{\theta}_{\rm opt} = -\frac{\mu}{\nu}\vec{\nabla}e, \tag{2}$$

as represented in Fig. 1(c).

Minimizing the tilt free energy density Eq. (1), the tilt effect of cell adhesion receptors results in the following free energy:

$$F_{\rm tilt} = \int {\rm d}^2\boldsymbol{x}\left[-\frac{1}{2}\sigma_a\phi(\nabla e)^2\right], \tag{3}$$

where $\sigma_a = \mu^2/\nu$ quantifies the tilt intensity. Equation (3) suggests that the tilt effect of cell adhesion receptors effectively contributes to a negative surface tension term $\sigma_{\rm tilt} = -\sigma_a\phi < 0$; the change of sign in the surface tension is reminiscent of Lifshitz points [30].

Adhesion.—Following Refs. [10,11], we assume that, in the presence of adhesion molecules, the membrane is pinned at a relatively short distance (∼20 nm) to the substrate, while in the absence of adhesion molecules, the membrane rests at a larger distance (∼100 nm), due to glycocalyx steric interactions in cells; see Fig. 1(b). Building upon Ref. [10], we propose the following generic free energy for such adhesion-mediated interaction between the membrane and a flat substrate:

$$F_{\rm adh} = \int {\rm d}^2\boldsymbol{x}\left\{\frac{1}{2}k(\phi)e^2 - k(\phi)e_0(\phi)e - h(\phi)\right\}, \tag{4}$$

where e_0 stands for the membrane rest-length height (as measured from the attached height), k for the membrane-substrate adhesion stiffness, and h for the chemical potential of receptor-substrate binding. Here, we focus on the case of a constant $k(\phi) = k_0$ and linear relations $e_0(\phi) = e_0(1-\phi)$ and $h(\phi) = h_\phi\phi$; see Fig. 1(d) for adhesion energy profiles (the homogeneous case shown). A homogeneous state $e(\boldsymbol{x}) \to 0$ represents a fully adhered membrane [$\phi(\boldsymbol{x}) \to 1$] and $e(\boldsymbol{x}) \to e_0$ for a fully de-adhered one [$\phi(\boldsymbol{x}) \to 0$]. Increasing the chemical potential h_ϕ shifts the energy minima from $\phi \approx 0$ to $\phi \approx 1$ (Fig. S3 and Movie S1 [16]).

Results.—We are interested in the minimum energy state of the system. We first consider the stability of homogeneous steady states, denoted $(\bar{e}, \bar{\phi})$. Solving for the condition $\delta F/\delta\phi = 0$, we find that the number of homogeneous states depends on the chemical potential h_ϕ and a nondimensional parameter:

$$\zeta = \frac{ak_0e_0^2}{k_BT}, \tag{5}$$

which quantifies the ratio of the membrane-substrate repulsion energy ($\sim ak_0e_0^2$) to the entropic energy ($\sim k_BT$).

For a high temperature or weak membrane-substrate adhesion stiffness, that is, $\zeta < \zeta^{\rm cr}$ with $\zeta^{\rm cr} = 4$, there exists one and only one homogeneous state, regardless of the value of h_ϕ (Supplemental Material [16], Sec. III). For a lower temperature or a stronger membrane-substrate adhesion stiffness, i.e., $\zeta > \zeta^{\rm cr}$, the situation depends on the

value of h_ϕ; a single homogeneous phase exists for either $h_\phi < h_\phi^{\mathrm{cr},1}$ (corresponding to a dilute phase, i.e., with $\phi \approx \exp[a(h_\phi - k_0 e_0^2)/(k_B T)] \approx 0$ and $e \approx e_0$) and for $h_\phi > h_\phi^{\mathrm{cr},2}$ (corresponding to a dense phase, with $\phi \approx 1 - \exp[-a h_\phi/(k_B T)] \approx 1$ and $e \approx 0$); $h_\phi^{\mathrm{cr},1}$ and $h_\phi^{\mathrm{cr},2}$ depend on ζ and $k_0 e_0^2$ (the membrane-substrate adhesion energy barrier) with $h_\phi^{\mathrm{cr},1} = k_0 e_0^2 g(\zeta)$ and $h_\phi^{\mathrm{cr},2} = k_0 e_0^2[1 - g(\zeta)]$, where $g(\zeta)$ is a dimensionless function of ζ, with values between by 0 and 1; in the low-temperature limit $\zeta \gg \zeta^{\mathrm{cr}}$, we find that $g \simeq (1 + \ln\zeta)/\zeta \to 0$ (see Supplemental Material [16], Sec. III).

Such behavior follows Landau's phenomenology of phase transitions. At low temperatures $T < T^{\mathrm{cr}}$ with T^{cr} defined in terms of ζ^{cr}, i.e., $T^{\mathrm{cr}} = a k_0 e_0^2/(k_B \zeta^{\mathrm{cr}}) = (1/4) a k_0 e_0^2/k_B$, an increase in h_ϕ leads to a first-order transition from a dilute (gaslike) phase to a dense (liquidlike) state (Fig. S3 [16]). Beyond the critical temperature T^{cr}, the system transitions to a disordered (gaslike) state (Figs. S3 and S4 and Movie S2 [16]). Such a liquid-gas paradigm is mentioned for cell adhesion binders in Refs. [8,31]; yet, as such, this cannot explain the formation of stable clusters.

For intermediate values $h_\phi^{\mathrm{cr},1} < h_\phi < h_\phi^{\mathrm{cr},2}$, three homogeneous states exist (Fig. S3 [16]), with a local maxima $(e_{\mathrm{med}}, \phi_{\mathrm{med}})$ and two local minima, i.e., the dilute and dense states, denoted $(e_{\max}, \phi_{\min})$ and $(e_{\min}, \phi_{\max})$, respectively. The free energy densities of these two energy minimum states are $f(e_{\max}; \phi_{\min}) \approx -k_0 e_0^2/2$ and $f(e_{\min}; \phi_{\max}) \approx -h_\phi$, respectively; thus,

$$h_\phi^{\mathrm{cr},3} = \frac{k_0 e_0^2}{2}, \tag{6}$$

which is the critical potential below which the dilute state is favored as compared to the dense one.

We next consider the dynamic stability of the homogeneous state $(\bar{e}, \bar{\phi})$, by examining the second-order variation of the total free energy, $\delta^2 F$, expressed in the Fourier space as $\delta^2 F = \int \mathrm{d}^2 \boldsymbol{q} \hat{\boldsymbol{\Phi}}(\boldsymbol{q}) \cdot \boldsymbol{J}(\boldsymbol{q}) \cdot \boldsymbol{\Phi}(\boldsymbol{q})/(2\pi)^2$, with $\boldsymbol{q}$ being the wave vector (for details, see Supplemental Material [16], Sec. III). The eigenvalues $\lambda_\pm(\boldsymbol{q})$ $(\lambda_- < \lambda_+)$ of the Jacobian matrix $\boldsymbol{J}(\boldsymbol{q})$ determine the dynamic stability of the homogeneous state, with $\mathrm{Re}(\lambda_\pm) > 0$ for a stable state.

Using this method, we find that the homogeneous dilute state $(e_{\max}, \phi_{\min})$ is stable for all wave vectors $\boldsymbol{q}$; in contrast, near the homogeneous dense state $(e_{\min}, \phi_{\max})$, the smaller eigenvalue reads $\lambda_- \simeq e_0^2[k_0 + (\sigma - \sigma_a) q^2 + \kappa q^4]$; the minimum of such an expression reads $\min_q\{\lambda_-\} = k_0 > 0$ for $\sigma_a < \sigma$ and $\min_q\{\lambda_-\} = k_0 - (\sigma_a - \sigma)^2/(4\kappa)$ for $\sigma_a > \sigma$. This leads to the following critical tilt intensity for instabilities to occur:

$$\sigma_a^{\mathrm{cr}} = \sigma + 2\sqrt{k_0 \kappa}, \quad \text{for } h_\phi > h_\phi^{\mathrm{cr},3}. \tag{7}$$

In the regime of $\sigma_a > \sigma_a^{\mathrm{cr}}$, the most unstable wave number is $q_{\min} = \sqrt{(\sigma_a - \sigma)/(2\kappa)}$. In particular, at the critical point $\sigma_a = \sigma_a^{\mathrm{cr}}$, the most unstable wave number reads $q^{\mathrm{cr}} = \sqrt[4]{k_0/\kappa}$, corresponding to the characteristic size of cluster formation:

$$\ell^{\mathrm{cr}} = 2\pi \sqrt[4]{\frac{\kappa}{k_0}}. \tag{8}$$

The analytical expressions of Eqs. (7) and (8) accurately predict the transitions in patterns observed through gradient-descent simulations; see Figs. 2(a) and S5 [16].

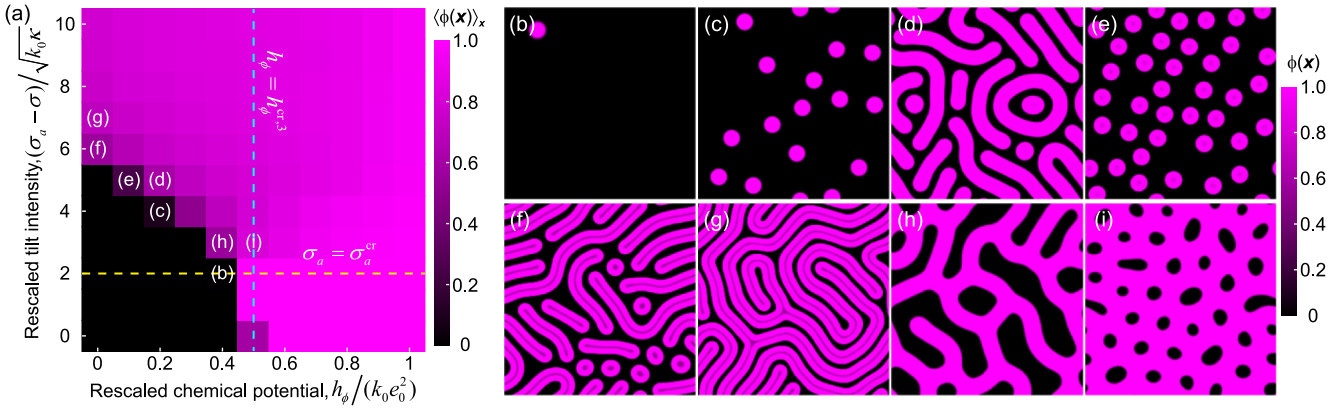

FIG. 2. (a) Diagram of the fraction of cell adhesion receptors averaged over the whole space (dark, $\langle\phi\rangle = 0$; light magenta, $\langle\phi\rangle = 1$) as a function of $h_\phi/(k_0 e_0^2)$ (i.e., the chemical potential to the membrane-substrate adhesion energy barrier ratio) and $(\sigma_a - \sigma)/\sqrt{k_0\kappa}$ (i.e., the tilt to attachment-induced bending surface tension ratio). The cyan dashed line represents the critical transition $[h_\phi = h_\phi^{\mathrm{cr},3}$; see Eq. (6)] from an unbound state to a bound state in the absence of the tilt effect. The yellow dashed line represents the critical transition $[\sigma_a = \sigma_a^{\mathrm{cr}}$; see Eq. (7)] from a fully bound pattern to a cross-linked pattern at a high chemical potential regime, $h_\phi > h_\phi^{\mathrm{cr},3}$. (b–i) Typical patterns of cell adhesion receptor clustering, where the color code corresponds to the fraction $\phi(\boldsymbol{x})$ of cell adhesion receptors at the position $\boldsymbol{x}$. See Table S1 in Supplemental Material [16] for parameter values.

Simulations.—We briefly sketch our numerical method (see Supplemental Material [16], Sec. III, for details). To reach the energy minimum, we consider the annealing dynamics $\dot{\phi} = -\delta F/\delta\phi$ and $\dot{e} = -\delta F/\delta e + \eta(\boldsymbol{x}, t)$, with a noise term $\eta(\boldsymbol{x}, t)$ whose amplitude decays with time [32]; we point out that the total number of adhesion molecules is not conserved through the simulation. We use the spectral method on a 256×256 two-dimensional lattice within a square domain of size $L = 1280$ nm (much larger than the typical size of integrin clusters $\ell \sim 100$ nm [12,13]) with periodic boundary conditions.

With no tilt coupling ($\sigma_a = 0$), increasing the chemical potential h_ϕ leads to a first-order-like transition from the dilute to dense homogeneous phases but does not result in stable cluster formation (Fig. S3 and Movie S1 [16]). In contrast, in the absence of adhesion ($k_0 = 0$ or $e_0 = 0$, and $h_\phi = 0$), a strong tilt effect is sufficient to destabilize the homogeneous state around $\phi \simeq 0.5$, but no circular clusters emerge; see Fig. S6 [16].

In the presence of tilt and adhesion, we identify two regimes depending on the value of h_ϕ with respect to a critical value $h_\phi^{\mathrm{cr},3}$. For $h_\phi > h_\phi^{\mathrm{cr},3}$, upon increasing σ_a beyond the value of σ_a^{cr} predicted by Eq. (7), dilute ($\phi \approx 0$) circular patches arise within the otherwise fully adherent state ($\phi \approx 1$). In contrast, for $h_\phi < h_\phi^{\mathrm{cr},3}$, dense circular patches (modeling clusters) emerge for $\sigma_a > \sigma_a^{\mathrm{cr}}$, where σ_a^{cr} now depends approximately linear on h_ϕ (Fig. 2). This results in the following overall expression for the critical tilt intensity: $\sigma_a^{\mathrm{cr}} = \sigma + 2\sqrt{k_0\kappa} + \omega\left(h_\phi^{\mathrm{cr},3} - h_\phi\right)\mathbb{1}(h_\phi < h_\phi^{\mathrm{cr},3})$, with $\omega \approx 6\sqrt{\kappa/k_0}/e_0^2$, as obtained by numerical estimate, and $\mathbb{1}$ is the indicative function. At $\sigma_a = \sigma_a^{\mathrm{cr}}$, hexagonally arranged circular clusters form; see Fig. 2. At higher σ_a values, the number of circular patches decreases due to the onset of long linear structures; at even larger σ_a values, these linear structures connect into domain-size, Turing-like patterns (Fig. S7 [16]).

Discussion.—Increasing σ_a leads to a behavior that resembles the dots to stripes transition observed in the Swift-Hohenberg model for convection patterns [33]; indeed, as discussed in Supplemental Material [16], Sec. III, we find that σ_a controls the bifurcation parameter value and a quadratic term is present within the nonlinear function.

Increasing the membrane tension σ leads to the disappearance of patterns, either in favor of the homogeneous dilute and detached state, for $h_\phi < h_\phi^{\mathrm{cr},3}$ [Figs. 1(e) and S9 [16]), or to the homogeneous dense and adhered state for $h_\phi > h_\phi^{\mathrm{cr},3}$ (Fig. S9 [16]), as sketched in Ref. [34].

Reducing the height difference e_0 between the adhered and detached state promotes the transition from circular dots to linear structures; see Fig. S8 [16].

Experimental relevance.—We consider a typical distance between binders $d = 10$ nm ($a = 100$ nm^2) [12]; a typical binding energy $k_0 e_0^2 a \sim 10 k_B T$ [10,11]; a typical height difference $e_0 = 80$ nm. With these values, we find that the ratio of the adhesion energy to the entropic energy $k_0 e_0^2/(k_B T/a) \sim 10$, hence satisfying $\zeta > \zeta^{\mathrm{cr}}$ (i.e., low-temperature case $T < T^{\mathrm{cr}}$). These estimates also fix the membrane-substrate adhesion stiffness at $k_0 \sim 10 k_B T/(e_0^2 a) \sim 10^{-5} k_B T \cdot \mathrm{nm}^{-4}$; the effective stiffness, $k_0 a \sim 10^{-3} k_B T \cdot \mathrm{nm}^{-2}$, is consistent with one provided in Ref. [10] (the parameter λ therein). Furthermore, considering $D_\phi = k_B T$, a typical cell membrane tension $\sigma = 2 \times 10^{-5}$ J $\cdot$ m$^{-2} \approx 0.005 k_B T \cdot \mathrm{nm}^{-2}$ [27,35], and membrane bending stiffness $\kappa = 10 k_B T$ [27,29,36], we find that adhesion is the dominant contribution to the critical tilt strength, with $\sigma_a^{\mathrm{cr}} \approx 7\sigma \approx 0.03 k_B T \cdot \mathrm{nm}^{-2}$.

Such critical tilt energy is accessible. Indeed, a $1 k_B T$ gain in conformational energy due to tilt corresponds to $\sigma_a \approx 0.1 k_B T \cdot \mathrm{nm}^{-2} \approx 3\sigma_a^{\mathrm{cr}}$, with a height gradient of order 1 (for integrins, the membrane height is approximatively 100 nm in the de-adhered state and 20 nm in the adhered state [10]). Such a typical tilt intensity is sufficient to generate stable clusters. With these values, we observe a typical cluster size $\ell^{\mathrm{sim}} \approx 100$ nm in simulations, in agreement with the size of integrin-based nascent adhesions [12].

Especially interesting is that the pattern predicted by our theory strongly resembles the shape and distribution of fibrillar adhesions in human umbilical vein endothelial cells (HUVEC); see Figs. 2(d), 2(f), and 3(a). In contrast, focal adhesions, shown in Fig. 3(b), do not resemble the pattern predicted by this theory and are most probably formed by a different mechanism. In contrast to focal

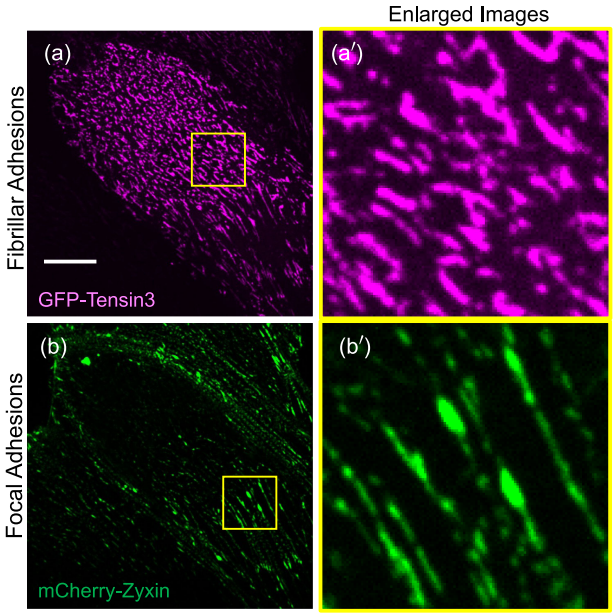

FIG. 3. Confocal image of integrin adhesions of a human umbilical vein endothelial cell (HUVEC), with fibrillar adhesions visualized by GFP-fused Tensin3 (a) and focal adhesions visualized by mCherry-fused Zyxin (b); (a′) and (b′) are magnified regions boxed in (a) and (b), respectively. Scale bar, 10 μm.

adhesions, fibrillar adhesions are also sensitive to different treatments affecting membrane tension (see Refs. [37,38]).

Extensions.—In our model, the membrane could include the cell cortex; yet, here we do not consider actin turnover and contractility explicitly. This is particularly justified for nascent adhesions, which form before any visible actin recruitment [12]. We also show that a biased averaged orientation, modeling the effect of a directed actin retrograde flow, favors the formation of oriented linear adhesions (Supplemental Material [16], Sec. V, Fig. S11). We also show clustering for a ϕ-dependent membrane-substrate adhesion stiffness $k(\phi)$ in Eq. (4) (see Supplemental Material [16], Sec. IV, Fig. S10).

Perspectives.—We envisage two adaptations of our work: (i) to describe binders between opposite free membranes and (ii) to account for a statistics of activation and deactivation, which modulate the affinity and shape of integrins [39].

Conclusion.—We propose tilt as a new paradigm explaining the stable clustering of cell adhesion receptors. Likely, recently developed polarization techniques will soon provide further means to challenge the tilt hypothesis [40].

J.-F. R. is hosted at the Laboratoire Adhésion Inflammation (LAI) and thanks fruitful discussions with Pierre-Henri Puech. The project leading to this publication has received funding from France 2030, the French Government program managed by the French National Research Agency (ANR-16-CONV-0001), and from the Excellence Initiative of Aix-Marseille University—A*MIDEX, ANR-20-CE30-0023 (COVFEFE) and ANR-21-CE13-0050 (CODAC). R. C. was supported by Singapore National Research Foundation's CRP grant (No. NRF2012NRF-CRP001-084). A. J. F. and A. D. B. research are supported by the Singapore Ministry of Education under the Research Centres of Excellence program through the Mechanobiology Institute at National University of Singapore (A-0003467-01-00 and A-0003467-00-00) and the Tier 3 grant (MOE-MOET32021), and by National Research Foundation (NRF) Singapore under its Mid-Sized Grant (NRF-MSG-2023-0001-0003).

*jacques.prost@curie.fr
†jean-francois.rupprecht@univ-amu.fr

[1] B. M. Gumbiner, Cell **84**, 345 (1996).
[2] B. Ladoux and A. Nicolas, Rep. Prog. Phys. **75**, 116601 (2012).
[3] U. S. Schwarz and S. A. Safran, Rev. Mod. Phys. **85**, 1327 (2013).
[4] Z. Sun, M. Costell, and R. Fässler, Nat. Cell Biol. **21**, 25 (2019).
[5] M. Janiszewska, M. C. Primi, and T. Izard, J. Biol. Chem. **295**, 2495 (2020).
[6] M. A. Al-Aghbar, A. K. Jainarayanan, M. L. Dustin, and S. R. Roffler, Commun. Biol. **5**, 40 (2022).
[7] S. A. Maynard, J. Ranft, and A. Triller, Nat. Rev. Neurosci. **24**, 422 (2023).
[8] R. Bruinsma and E. Sackmann, C. R. Acad. Sci. **2**, 803 (2001).
[9] S. Schumacher, D. Dedden, R. V. Nunez, K. Matoba, J. Takagi, C. Biertümpfel, and N. Mizuno, Sci. Adv. **7**, eabe9716 (2021).
[10] T. Bihr, U. Seifert, and A.-S. Smith, Phys. Rev. Lett. **109**, 258101 (2012).
[11] T. Bihr, U. Seifert, and A.-S. Smith, New J. Phys. **17**, 083016 (2015).
[12] R. Changede, X. Xu, F. Margadant, and M. Sheetz, Dev. Cell **35**, 614 (2015).
[13] R. Changede, H. Cai, S. J. Wind, and M. P. Sheetz, Nat. Mater. **18**, 1366 (2019).
[14] B. Geiger, A. Bershadsky, R. Pankov, and K. M. Yamada, Nat. Rev. Mol. Cell Biol. **2**, 793 (2001).
[15] G. Mana, D. Valdembri, J. A. Askari, Z. Li, P. Caswell, C. Zhu, M. J. Humphries, C. Ballestrem, and G. Serini, Life Sci. Alliance **6**, e202201388 (2023).
[16] See Supplemental Material at http://link.aps.org/supplemental/10.1103/PhysRevLett.132.188402, which provides further details of the theoretical model, analytical calculations, and numerical simulations and includes Refs. [17–24].
[17] R. B. Hoyle, *Pattern Formation: An Introduction to Methods* (Cambridge University Press, Cambridge, England, 2006).
[18] G. Popescu, T. Ikeda, K. Goda, C. A. Best, M. Laposata, S. Manley, R. R. Dasari, K. Badizadegan, and M. S. Feld, Phys. Rev. Lett. **97**, 218101 (2006).
[19] A.-S. Smith, K. Sengupta, S. Goennenwein, U. Seifert, and E. Sackmann, Proc. Natl. Acad. Sci. U.S.A. **105**, 6906 (2008).
[20] X.-P. Xu, E. Kim, M. Swift, J. Smith, N. Volkmann, and D. Hanein, Biophys. J. **110**, 798 (2016).
[21] V. Swaminathan, J. M. Kalappurakkal, S. B. Mehta, P. Nordenfelt, T. I. Moore, N. Koga, D. A. Baker, R. Oldenbourg, T. Tani, S. Mayor, T. A. Springer, and C. M. Waterman, Proc. Natl. Acad. Sci. U.S.A. **114**, 10648 (2017).
[22] M. L. Gardel, I. C. Schneider, Y. Aratyn-Schaus, and C. M. Waterman, Annu. Rev. Cell Dev. Biol. **26**, 315 (2010).
[23] K. Jansen, P. Atherton, and C. Ballestrem, Semin. Cell Dev. Biol. **71**, 75 (2017).
[24] Y. Wu and S. X. Sun, Biophys. J. **122**, 3354 (2023).
[25] M. L. Huggins, J. Chem. Phys. **9**, 440 (1941).
[26] P. J. Flory, J. Chem. Phys. **9**, 660 (1941).
[27] I. Raote, M. Chabanon, N. Walani, M. Arroyo, M. F. Garcia-Parajo, V. Malhotra, and F. Campelo, eLife **9**, e59426 (2020).
[28] W. Helfrich, Z. Naturforsch. C **28**, 693 (1973).
[29] T. R. Weikl, Annu. Rev. Phys. Chem. **69**, 521 (2018).
[30] R. M. Hornreich, M. Luban, and S. Shtrikman, Phys. Rev. Lett. **35**, 1678 (1975).
[31] F. Brochard-Wyart and P. G. de Gennes, Proc. Natl. Acad. Sci. U.S.A. **99**, 7854 (2002).
[32] P. J. M. van Laarhoven and E. H. L. Aarts, *Simulated Annealing: Theory and Applications* (Springer, New York, 1987).

[33] J. Swift and P. C. Hohenberg, Phys. Rev. A **15**, 319 (1977).
[34] H. Delanoë-Ayari, R. A. Kurdi, M. Vallade, D. Gulino-Debrac, and D. Riveline, Proc. Natl. Acad. Sci. U.S.A. **101**, 2229 (2004).
[35] M. M. Kozlov and L. V. Chernomordik, Curr. Opin. Struct. Biol. **33**, 61 (2015).
[36] J. Steinkühler, E. Sezgin, I. Urbančič, C. Eggeling, and R. Dimova, Commun. Biol. **2**, 337 (2019).
[37] N. B. M. Rafiq, G. Grenci, C. K. Lim, M. M. Kozlov, G. E. Jones, V. Viasnoff, and A. D. Bershadsky, Phil. Trans. R. Soc. B **374**, 20180228 (2019).
[38] A. J. Farrugia and A. Bershadsky (unpublished).
[39] L. Limozin and P.-H. Puech, J. Membr. Biol. **252**, 397 (2019).
[40] V. Curcio, L. A. Alemán-Castañeda, T. G. Brown, S. Brasselet, and M. A. Alonso, Nat. Commun. **11**, 5307 (2020).